Photodissociation dynamics of HN_3. The N_3 fragment internal energy distribution

Tobias Haas, Karl-Heinz Gericke, Christof Maul and Franz Josef Comes

Institut für Physikalische und Theoretische Chemie, Universität Frankfurt am Main, W-6000 Frankfurt am Main 50, Germany

Received 17 August 1992; in final form 6 November 1992

The H-atom velocity distribution of the photofragmentation of HN_3 at 243 nm has been characterized using resonant enhanced multiphonon ionisation (REMPI) in combination with time-of-flight (TOF) measurements. The internal energy distribution of the N_3 fragment has been determined from the experimental results. The structures in the N_3 internal energy distribution were assigned to the excitation of the N_3 symmetric stretching mode. The relative population of the (000) : (100) : (200) : (300) : (400) modes was found to be 0.09 : 0.19 : 0.28 : 0.29 : 0.15. The means of the vibrational and rotational energies are $\langle E_{vib} \rangle = 2970\ cm^{-1}$ and $\langle E_{rot} \rangle = 720\ cm^{-1}$. The excitation of the symmetric stretching mode indicates the dominating influence of the N–N_2H, N_2–NH, and N_3–H coordinates of the upper potential energy surface (PES) on the N_3 internal energy distribution.

1. Introduction

The photodissociation of HN_3 has been object of extensive studies by several groups [1–9]. In an infrared multiphoton dissociation experiment Casassa et al. [1–3] observed the NH product in the $X\,^3\Sigma^-$ and the $a\,^1\Delta$ quantum state depending on the applied IR wavelength. Several studies [4–9] were carried out by excitation of the $\tilde{A}\,^1A''$ state of the HN_3 molecule using various UV wavelengths. Scalar properties as well as vector correlations have been determined giving a detailed view into the dissociation dynamics of the reaction

$$HN_3 + h\nu \rightarrow NH(a\,^1\Delta) + N_2(X\,^1\Sigma_g^+) .$$

Another reaction channel leading to H atoms has recently been verified [10] by the detection of nascent H atoms using photolysis wavelengths of 193 and 248 nm. Two reaction paths leading to the separation of a H atom are energetically possible, although the second one is spin-forbidden:

$$HN_3 + h\nu \rightarrow H(^2S) + N_3(^2\Pi) ,$$

$$HN_3 + h\nu \rightarrow H(^2S) + N(^4S) + N_2(X\,^1\Sigma_g^+) .$$

In a recent study some scalar properties as well as the asymmetry ($\langle \mu \cdot v \rangle$ correlation) of the nascent H atom have been determined at photolysis wavelengths of 248 and 193 nm using the sub-Doppler laser-induced fluorescence (LIF) technique [11]. If the available energy is increased by decreasing the photolysis wavelength, the additional energy is released as internal energy of the N_3 fragment. The strongly negative $\langle \mu \cdot v \rangle$ correlation suggests that the fragments are ejected in the molecular plane. The N_3 fragment is believed to be highly vibrationally excited but rotationally cold since the N_3 chain in the HN_3 is elongated compared to the free N_3 radical. In the present work, we intend to classify which internal modes are excited in the dissociation process in order to determine which molecular coordinates are involved in this elementary reaction.

The N_3 radical has already been observed by the LIF technique [12,13] as a product of the photolysis of HN_3. But it was believed to be produced by the secondary reaction $HN_3 + NH(a\,^1\Delta) \rightarrow NH_2 + N_3$ [12]. Unfortunately the $\tilde{A}\,^2\Sigma$ state of the N_3 molecule used for the LIF detection is predissociative [12,14], and so the sensitivity of this experimental technique is drastically reduced, making it difficult to detect low N_3 concentrations. Other than this, several thousand rovibronic states can be populated by the N_3 fragment within a range of 5000 cm^{-1} internal energy [15], so the expected concentration per

quantum state is low. Moreover, only a few of the vibrational bands [12,13,16] have been resolved until now. Thus the LIF technique is not an appropriate tool for investigating the nascent N_3 product.

The easiest way to obtain information about the population of quantum states of the N_3 fragment is the determination of the H atom kinetic energy distribution which reflects the internal energy distribution of the N_3 fragment.

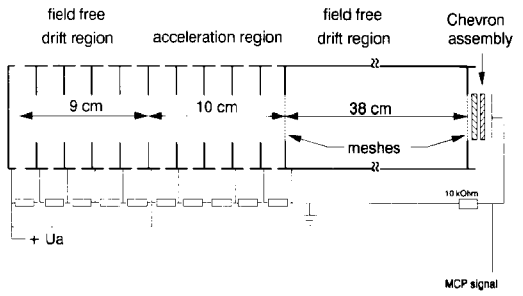

Fig. 1. Schematic diagram of the TOF spectrometer.

2. Experimental

The H-atom velocity distribution is analyzed with the (2+1)-REMPI-TOF technique [17–19] as a diagnostic tool. Because the influence of initial parent molecule motion has to be minimized, the use of supersonic expansion in a molecular beam is necessary. The reaction chamber is made of stainless steel and evacuated by two baffled 500 ℓ/s oil diffusion pumps to a base pressure of 10^{-4} Pa. The home-built TOF spectrometer is mounted inside the reaction chamber and evacuated by a 360 ℓ/s turbomolecular pump (Leybold Heraeus 360 CSV).

HN_3 is generated by dropwise addition of phosphoric acid to NaN_3 under vacuum and stored in a glass bulb at a maximum pressure of 10^4 Pa. The HN_3 is expanded through a pulsed nozzle (General Valve) into the reaction chamber. The molecular beam is collimated by a skimmer before it enters the TOF spectrometer, where it is intersected by the photolyzing/analyzing laser beam. During the measurements the background pressure is 10^{-3} Pa in the TOF tube.

The (2+1) REMPI process uses the $H(2\,^2S) \leftarrow H(1\,^2S)$ resonant transition as an intermediate step. The photolyzing and analyzing light is delivered by an excimer laser pumped (LPX 605i Lambda Physik) dye laser system with SHG (LPD-3000 Lambda Physik) and focused tightly into the spectrometer by a 6 cm quartz lens. The laser power is carefully controlled to avoid space charge effects and is typically kept below 1 mJ. H ions are detected by a double stage multichannel plate (MCP) assembly (Galileo).

The TOF spectrometer (fig. 1) is designed for maximum kinetic energy resolution. All metal parts inside the spectrometer are gold plated to avoid disturbing electric fields due to anisotropic work functions [11]. The spectrometer is divided into three parts: a 9 cm long drift region, a 10 cm long acceleration region, and a second 38 cm long drift region which is separated from the acceleration region and the MCP assembly by two gold plated stainless steel meshes. TOF drift profiles were obtained by applying an electric field between the last six electrodes, so that the H ions are produced in a field free region. Therefore, only ions which initially fly directly towards the detector will hit the detector. In this operation mode only a few ions will reach the MCP assembly, resulting in a weak H ion signal. Therefore an amplifier/discriminator unit (7011 FAST) in combination with a multihit time to digital converter (7885 FAST) has been used to process the signal. The TOF signal is obtained by adding over a large number (10^3–10^5) of laser shots. The advantage of this operation mode is a high resolution of the H atom recoil velocity distribution.

To compensate for any systematic errors due to inhomogeneous electric fields inside the TOF spectrometer, the H atom velocities were calibrated by observing H atoms produced in the following reaction:

$$HI + h\nu(243\,\text{nm}) \rightarrow H(^2S) + I(^2P_{3/2}) ,$$

$$HI + h\nu(243\,\text{nm}) \rightarrow H(^2S) + I^*(^2P_{1/2}) .$$

Since the dissociation energy [20] of HI and the spin orbit splitting of the I atom are well known it is possible to calculate the two discrete H atom recoil velocities belonging to the different I states.

3. Results and discussion

To obtain precise information on the H atom ve-

locity distribution which represents the N_3 internal energy distribution, several TOF drift profiles were recorded. A typical TOF drift profile is shown in fig. 2 which was obtained by accumulation over 5×10^5 laser shots.

The relation between the H atom velocity and the measured time of flight is given to a good approximation by

$$t(v_H)=t_c+d/v_H\,, \tag{1}$$

where d is the distance between the laser focus and the beginning of the acceleration region. The constant t_c accounts for the time of flight between the beginning of the acceleration region and the MCP assembly. In our experiment t_c is assumed to be independent of v_H since the additional kinetic energy of the acceleration (109 eV) is much larger than the kinetic energy release in the photodissociation (≈ 1 eV).

The system is calibrated with HI as a standard to evaluate the constant t_c. The conversion of the TOF drift profile into a H atom kinetic energy spectrum is shown in fig. 3 where the following equation has been used:

$$E_{kin}(H)=\tfrac{1}{2}m_H\{d/[t(v_H)-t_c]\}^2\,. \tag{2}$$

The intensity normalization was carried out using the relation $f(E)\,dE=f(t)\,dt$.

Since linear momentum has to be conserved, the total kinetic energy of both fragments is given by

$$E_{kin}(tot)=E_{kin}(H)(1+m_H/m_{N_3})\,. \tag{3}$$

So the internal energy distribution of the N_3 fragment can be calculated from the total kinetic energy distribution to be

$$E_{int}(N_3)=E_{av}-E_{kin}(tot)\,. \tag{4}$$

E_{av} is the available energy for the products, $E_{av}=h\nu+E_{int}(HN_3)-E_{diss}$, where E_{diss} is the dissociation energy of the H–N_3 bond, and $E_{int}(HN_3)$ is the internal energy of the parent molecule which is negligible since HN_3 is cooled in a molecular beam.

It can be seen from fig. 3 that the observed H atom kinetic energy distribution consists of five nearly equally spaced maxima which are well fitted by the sum of five Gaussian functions of the same width:

$$I=B+\sum_{i=0}^{4}A_i\exp\left[-4\ln 2\left(\frac{E_{kin}(H)-E_{kin,i}(H)}{\Delta E_{kin}(H)}\right)^2\right]. \tag{5}$$

B is the height of the baseline, the factors A_i are the intensities, $E_{kin,i}(H)$ are the center positions, and $\Delta E_{kin}(H)$ is the common width (fwhm) of the five

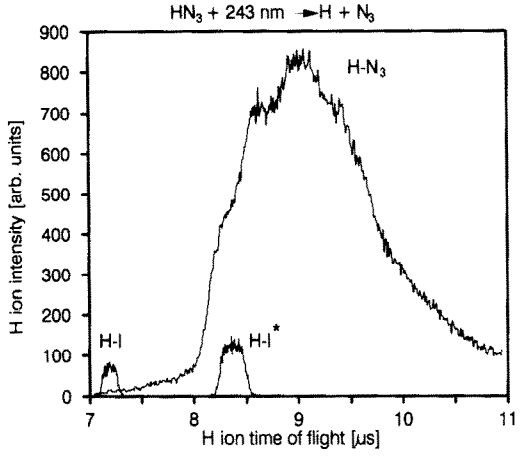

Fig. 2. TOF drift spectra of H ions generated in the HN_3 (upper curve), and HI (lower curve) photodissociation/ionization at 243.12 nm. The H signals generated by the photolysis of HI were used for velocity calibration.

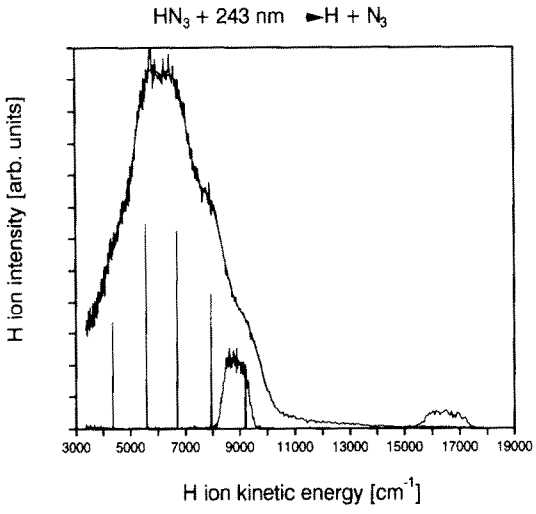

Fig. 3. H atom kinetic energy distribution of the HN_3 photolysis at 243.12 nm. The solid line is a least-squares fit of eq. (5). The five markers indicate the height and position of each Gaussian function. The lower curve represents the H atom kinetic energy distribution of the HI photolysis at 243.12 nm, from which the width of the response function was obtained.

Gaussian functions. The results of the fitting procedure are summarized in table 1.

The tail of fast H atoms in fig. 3 with kinetic energy of more than 11000 cm^{-1} can be assigned to a minor secondary dissociation of $NH(a^1\Delta)$ fragments into $N(^2D)$ and $H(^2S)$. However, the internal state distribution and the kinetic energy distribution of the $NH(a^1\Delta)$ product from the 248 nm photolysis [8,21] suggest an almost constant background signal of H atoms due to secondary processes in the kinetic energy range under consideration falling off to zero at 3000 cm^{-1} respectively at 14000 cm^{-1}. Therefore the height of the baseline B is set approximately equal to the value at the edge of the profile of fig. 3 at 11000 cm^{-1}. This procedure is justified by the fact that within the experimental error it yields the same values for the mean fragment energies as the preceding experiments by Lock et al. [11] where secondary dissociation can be excluded.

In order to obtain the dissociation energy $E_{diss}(H\text{–}N_3)$ it is necessary to determine the maximum H atom kinetic energy $E_{kin,max}(H)$ from these fitted spectra. Since the data shown in fig. 3 are a convolution of the H atom kinetic energy spectra with the response function of the TOF spectrometer, one has to consider the width of the response function for a correct evaluation of the maximum H-atom kinetic energy. Assuming the response function to be Gaussian with a width of ΔE_{resp} and the kinetic energy distribution to be described by eq. (5), the maximum H-atom kinetic energy is given by

$$E_{kin_{max}}(H) = E_{kin,0}(H) + (1 + 1/\sqrt{e})\sigma , \qquad (6)$$

where $E_{kin,0}(H)$ is taken from the fitting procedure (eq. (5)) and σ is given by

$$\sigma = [(\Delta E_{kin}(H)^2 - \Delta E_{resp}^2)/(4 \ln 2)]^{1/2} . \qquad (7)$$

Since the dissociation of jet-cooled HI leads to monoenergetic H atoms, the observed signal can directly be regarded as the response function of the spectrometer. The width of the response function was determined to be ≈ 950 cm^{-1} by evaluating the width of the H atom calibration signal from the HI photolysis. A value of 10270 cm^{-1} was obtained for $E_{kin,max}(H)$. Assuming that H atoms with maximum kinetic energy can be correlated with N_3 fragments having zero internal energy and, if furthermore no internal energy for the HN_3 molecule is considered, we can write

$$E_{diss}(H\text{–}N_3) = h\nu - E_{kin,max}(H)(1 + m_H/m_{N_3}) . \qquad (8)$$

The value obtained for $E_{diss}(H\text{–}N_3) = 30850 \pm 400$ cm^{-1} is in good agreement with previous measurements [11]. The error is mainly due to the response function regarded as Gaussian shaped which is a fairly crude approximation.

The H atom kinetic energy distribution can be converted into the N_3 internal energy distribution (fig. 4) using eq. (4). The detected structure in the N_3 internal energy distribution already gives a hint on the energy release, e.g. the internal motion of the N_3 fragment. First of all, the measured energy dis-

Table 1
Positions ($E_{kin,i}(H)$), intensities (A_i), and width ($\Delta E_{kin}(H)$) of the five maxima in the H-atom kinetic energy distribution. $E_{in}(N_3)$ is the related internal energy of the N_3 fragment. All energies are given in wavenumbers

i	A_i	$E_{kin,i}(H)$	$E_{int}(N_3)$	$\Delta E_{kin}(H)$
0	0.09	9210	890	1270
1	0.19	7940	2200	1270
2	0.28	6700	3470	1270
3	0.29	5590	4610	1270
4	0.15	4350	5870	1270

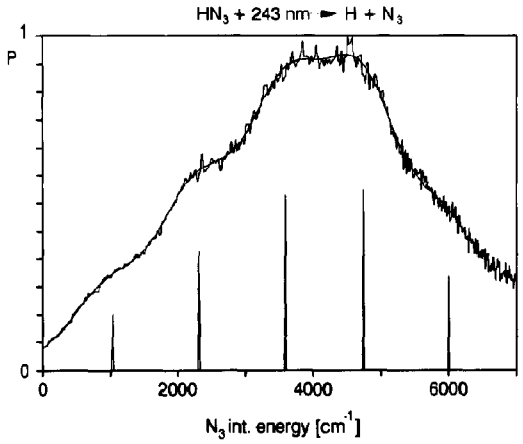

Fig. 4. Internal energy distribution of the N_3 fragment generated in the photolysis of HN_3 at 243.12 nm. The solid line is the least-squares fit of the H atom kinetic energy distribution (eq. (5)) after transformation into the N_3 internal energy distribution (eq. (4)). The five markers indicate the height and position of each Gaussian function.

tribution can hardly be attributed to pure rotational excitation of N_3, because we would not expect to see structure unless well separated selected groups of rotational states would be populated, which is unlikely. It remains that the observed structure is essentially from vibrational excitation of the N_3 product. Here again, pure excitation of the degenerated ν_2 bending mode cannot be attributed to the observed N_3 energy distribution, because one quantum of vibrational energy of the ν_2 mode carries 457 cm^{-1} [13] which is also far too low to be resolved in this experiment. Thus, only the N_3 stretching modes are responsible for the structured N_3 internal energy distribution. In order to discriminate between the symmetric stretch, $\nu_1 = 1320$ cm^{-1}, and the asymmetric stretch, $\nu_3 = 1644$ cm^{-1}, a quantitative analysis of the TOF spectra is necessary.

With the positions of $E_{kin,i}(H)$ and the intensities A_i of the five maxima of the kinetic energy distribution (fig. 3) one can calculate the position and the height of each maximum (table 1) in the N_3 internal energy distribution (fig. 4). The energy differences between the peaks are indicative for the type of stretching mode. Table 2 lists the possible vibrational modes, their energy and the remaining rotational energy of each maximum of the N_3 internal energy distribution [15]. Excitation of the asymmetric stretching mode (table 2, record 1) cannot explain the internal energy distribution of the N_3 fragment, since in that case the vibrational energy exceeds the observed N_3 internal energy. By the same argument, excitation of a combination mode consisting of a bending mode and several symmetric stretching vibrations (table 2, record 2) can be excluded. Only the excitation of the symmetric stretching mode (table 2, record 3) leads to a reasonable energy for the N_3 rotation. However, it should be mentioned that excitation of at most one quantum of the ν_3 mode (table 2, record 4) cannot be excluded. So it is evident that excitation of the ν_1 mode is responsible for the structures of the N_3 internal energy distribution. The population of the symmetric stretching mode is shown in fig. 5. If we assume an exclusive excitation of the ν_1 mode, then the mean vibrational energy is given by:

Table 2
Energies (cm^{-1}) of selected vibrational modes of the $N_3(^2\Pi)$ molecule [15]. The vibrational energies E_{vib} are averaged over the different spin states and the Renner–Teller splitting. Only those vibrational modes which yield a positive value for the remaining energy $E_{rem}(N_3)$ can explain the experimental results

Record	Vib. mode ($\nu_1\nu_2\nu_3$)	E_{vib}	$E_{rem}(N_3)$
1	000	35	860
	001	1680	520
	002	3330	140
	003	4980	−370
	004	6630	−760
2	010	570	320
	110	1890	310
	210	3210	260
	310	4530	−80
	410	5850	20
3	000	35	860
	100	1360	840
	200	2680	790
	300	3990	620
	400	5320	550
4	000	35	860
	001	1680	530
	101	2980	490
	201	4240	370
	301	5500	370

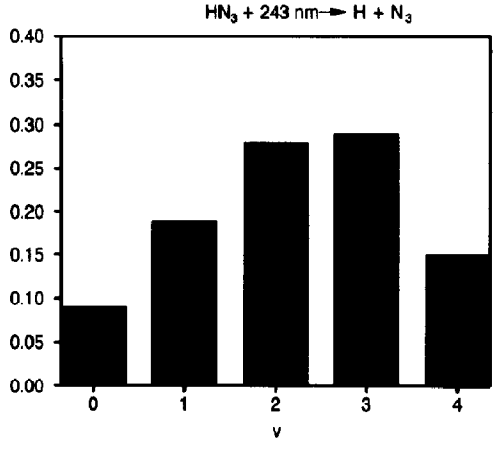

Fig. 5. The relative population of the ν_1 mode of the N_3 fragment generated by the photolysis of HN_3 at 243.12 nm.

$$\langle E_{\mathrm{vib}}(N_3)\rangle = \sum_{i=0}^{4} A_i E_{\mathrm{vib}}(i,0,0)$$

$$\approx 2970\ \mathrm{cm}^{-1}. \qquad (9)$$

The mean remaining rotational energy $\langle E_{\mathrm{rot}}(N_3)\rangle$ is determined to be 720 cm^{-1} where the values of record 3 in table 2 have been used. The partitioning of the available energy is calculated to be: $f_{\mathrm{trans}}=0.64$, $f_{\mathrm{vib}}=0.29$, and $f_{\mathrm{rot}}=0.07$.

A significant amount of rotational motion will broaden the width $\Delta E_{\mathrm{kin}}(H)$ of the kinetic energy distribution. If we compare the value $\Delta E_{\mathrm{kin}}(H) = 1270\ \mathrm{cm}^{-1}$ obtained by the fitting procedure with the width of the response function ΔE_{resp}, we can estimate the width of the rotational energy distribution ΔE_{rot}:

$$\Delta E_{\mathrm{rot}} = [\Delta E_{\mathrm{kin}}(H)^2 - \Delta E_{\mathrm{resp}}^2]^{1/2}$$

$$\approx 840\ \mathrm{cm}^{-1}, \qquad (10)$$

where the response function and the internal energy distribution of a single stretching mode are assumed to be Gaussian.

For dynamical calculations it is of advantage to use Jacobian coordinates to describe the photodissociation process. However, the upper PES can be visualized easier when normal modes are used for a qualitative description of the fragmentation process of HN_3. The rotational excitation of the N_3 product is related to initial motion of the parent and to the torque provided by the gradient of the upper PES with respect to the NNH bending angle which describes the ν_4 mode of the parent. A strong N_3 rotation could be induced by a ν_4 bending motion of the NNH frame. Since the energy release in rotation is relatively low, the NNH bending angle dependence of the upper PES should be similar to that of the ground state. This is confirmed by ab initio calculations [22].

If the upper PES causes only a separation of the two products, i.e. the dissociation process is characterized by the Franck–Condon limit, then the release of the available energy in kinetic and internal energy of the N_3 fragment is determined by the quantum state distribution of the HN_3 parent molecule in its ground state and the internal energy distribution of the N_3 fragment should be nearly independent of the photolysis wavelength. Thus any additional available energy should be released as kinetic energy of the fragments. Since the N_3 fragment is a linear and symmetric molecule (N–N bond length 118 pm) and the HN_3 molecule has two different N–N bonds (113 and 124 pm), one would also expect an excitation of the N_3 asymmetric stretching mode from this asymmetrically elongated N_3 frame. Comparison of the experimental results with the predictions of the Franck–Condon limit indicates that the dissociation process cannot be described by the Franck–Condon limit because:

(1) the N_3 fragment is strongly excited [11],

(2) any additional available energy is released as internal energy of the N_3 fragments [11], and

(3) the symmetric stretching mode of the N_3 fragment is excited.

Thus the experimental data suggest that the photofragmentation process can be described by the strong coupling case, i.e. the motion of the fragments is essentially determined by the upper PES of the $\tilde{A}\,^1A''$ state and only to a minor extent by the ground state distribution of the HN_3 parent. So we expect steep gradients along the coordinates which lead to excitation of the ν_1 mode.

The fragmentation process is governed by anharmonic coupling phenomena on the upper PES. In a simplified mechanistic picture of the dissociation process this may be described in such a way that the original N_1–N_2 bond length of 113 pm is prolonged to 124 pm, or the N_2–N_3 bond length is compressed to 113 pm before complete fragmentation into $H+N_3$ in order to explain the observed N_3 symmetrical stretching vibration in the dissociation of the asymmetrical elongated N_1–N_2–N_3 chain of the N_1–N_2–N_3–H parent. The observed ν_1 vibrational distribution is centered around $v_1=2$. A quantum-mechanical calculation of the maxima of the $|\Psi|^2$ function, describing harmonic N_3 vibrations, shows that the N–N bond length of the free N_3 molecule is changed by about 6 pm for $v_1=2$ relative to the $|\Psi|^2$ maximum of the $v_1=0$ state. This shift in the bond length is necessary when the N_1–N_2–N_3 frame of the parent is "transformed" into the free N_3 product. The dissociation process may be visualized as follows:

While the H atom is recoiling from the neighboring N atom, this N atom approaches the N_1–N_2 frame to a distance of about 113 pm. During this approach the length (113 pm) of the strong N_1–N_2 bond should

not be changed significantly. When the symmetrical configuration of the N_1–N_2–N_3 frame is reached the influence of the recoiling hydrogen becomes negligible resulting in symmetrical vibrational motion of the N_3 product. Less likely is a fragmentation process which involves lengthening of the N_1–N_2 bond length to about 124 pm while the N_2–N_3 bond length remains essentially unchanged when the H atom is leaving the excited HN_3 complex. The influence of the hydrogen becomes unimportant for the fragmentation process when a symmetrical N_1–N_2–N_3 configuration is reached and the ν_1 mode of the product is excited.

Acknowledgement

This project was supported by the Deutsche Forschungsgemeinschaft and the German Fonds der Chemischen Industrie.

References

[1] J.C. Stephenson, M.P. Casassa and D.S. King, J. Chem. Phys. 89 (1988) 1378.
[2] B.R. Foy, M.P. Casassa, J.C. Stephenson and D.S. King, J. Chem. Phys. 89 (1988) 608; 90 (1989) 7037; 92 (1990) 2782.
[3] M.P. Casassa, B.R. Foy, J.C. Stephenson and D.S. King, J. Chem. Phys. 94 (1991) 250.
[4] A.P. Baronavski, R.G. Miller and J.R. McDonald, Chem. Phys. 30 (1978) 119.
[5] J.-J. Chu, P. Marcus and P.J. Dagdigian, J. Chem. Phys. 93 (1990) 257.
[6] K.-H. Gericke, R. Theinl and F.J. Comes, Chem. Phys. Letters 164 (1990) 605.
[7] K.-H. Gericke, R. Theinl and F.J. Comes, J. Chem. Phys. 92 (1990) 6548.
[8] K.-H. Gericke, T. Haas, M. Lock, R. Theinl and F.J. Comes, J. Phys. Chem. 95 (1991) 6104.
[9] K.-H. Gericke, M. Lock, R. Fasold and F.J. Comes, J. Chem. Phys. 96 (1992) 422.
[10] K.-H. Gericke, M. Lock and F.J. Comes, Chem. Phys. Letters 186 (1991) 427.
[11] M. Lock, K.-H. Gericke, T. Haas, C. Maul and F.J. Comes, to be published.
[12] T. Haas and K.-H. Gericke, Ber. Bunsenges. Physik. Chem. 95 (1991) 1289.
[13] R.A. Beaman, T. Nelson, D.S. Richards and D.W. Setser, J. Phys. Chem. 91 (1987) 6090.
[14] R.E. Continetti, R.R. Cyr, R.B. Metz and D.M. Neumark, Chem. Phys. Letters 182 (1991) 402.
[15] G. Chambaud and P. Rosmus, J. Chem. Phys. 96 (1992) 1.
[16] A.E. Douglas and W.J. Jones, Can. J. Phys. 43 (1965) 2216.
[17] T.A. Spiglanin, R.A. Perry and D.W. Chandler, J. Phys. Chem. 90 (1986) 6184.
[18] M. Mons and I. Dimicoli, J. Chem. Phys. 90 (1989) 4037.
[19] X. Xie, L. Schnieder, H. Wallmeier, R. Boettner, K.H. Welge and M.N.R. Ashfold, J. Chem. Phys. 92 (1990) 1608.
[20] R.D. Clear, S.J. Riley and K.R. Wilson, J. Chem. Phys. 63 (1975) 1340.
[21] F. Rohrer and F. Stuhl, J. Chem. Phys. 88 (1988) 4788.
[22] U. Meier and V.S. Staemmler, J. Phys. Chem. 95 (1991) 6112.